Chapter 7

On the formation of continental silicic melts in thermo-chemical mantle convection models: implications for early Earth and Venus

Abstract

Important constituents of Archean cratons, formed in the early and hot history of the Earth, are TTG plutons and greenstone belts. The formation of these granite-greenstone terrains is often ascribed to plate-tectonic processes. Buoyancy considerations, however, do not allow plate tectonics to take place in a significantly hotter Earth. We therefore propose an alternative mechanism for the coeval and proximate production of TTG plutons and greenstone-like crustal successions: When a locally anomalously thick basaltic crust has been produced by continued addition of extrusive or intrusive basalts due to partial melting of the underlying convecting mantle, the transition of a sufficient amount of basalt in the lower crust to eclogite may trigger a resurfacing event, in which a complete crustal section of over 1000 km long sinks into the mantle in less than 2 million years. Pressure release partial melting in the complementary upwelling mantle produces large volumes of basaltic material replacing the original crust. Partial melting at the base of this newly produced crust may generate felsic melts that are added as intrusives and/or extrusives to the generally mafic crustal succession, adding to what resembles a greenstone belt. Partial melting of metabasalt in the sinking crustal section produces a significant volume of TTG melt that is added to the crust directly above the location of 'subduction', presumably in

This chapter has been submitted by P. van Thienen, A.P. van den Berg and N.J. Vlaar for publication in *Tectonophysics*.

the form of a pluton. This scenario is self-consistently produced by numerical thermo-chemical mantle convection models, presented in this paper, including partial melting of mantle peridotite and crustal (meta-)basalt. The metamorphic p, T-conditions under which partial melting of metabasalt takes place in this scenario are consistent with geochemical trace element data for TTG's, which indicate melting under amphibolite rather than eclogite facies. Other geodynamical settings which we have also investigated, including partial melting in small scale delaminations of the lower crust, at the base of a anomalously thick crust and due to the influx of a lower mantle diapir fail to reproduce this behaviour unequivocally and mostly show melting of metabasalt in the eclogite stability field instead. The resurfacing scenario may also have been important in Venus' history, but probably did not produce significant volumes of continental material due to the dryness of this planet.

7.1 Introduction

The finding of detrital zircons up to 4.4 Gyr old, less than 200 million years after the accretion of the Earth, provides evidence that continental crust was already produced at this time (Peck et al., 2001). Growth curves for the continental crust, derived from isotopic analyses of rocks from Archean to present age, also indicate that the formation of continental crust may have started before 4.0 Ga (e.g. Taylor and McLennan, 1985; McCulloch and Bennett, 1994). In the recent Earth, most continental growth is accommodated by the accretion of volcanic arcs, which are formed by partial melting of the mantle wedge above subducting slabs, and intraplate volcanism, associated with hotspots. The material thus produced is on average of basaltic composition, but the continental crust has an andesitic bulk composition (Rudnick, 1995). In Archean cratons, a large fraction of the material consists of Tonalite-Trondhjemite-Granodiorite (TTG) suites, either metamorphosed to amphibolite facies gneiss-migmatites, or as plutons (Goodwin, 1991). Melting experiments indicate that these TTG's may have been formed by partial melting of hydrous metabasalts (eclogites or amphibolites) at pressures between 8 and 32 (optimally 22) kbar (Rapp et al., 1991). The presence of some water is required to lower the melting temperature to plausible values. The required conditions for this process may be found in subduction zone settings, but not exclusively (Rapp et al., 1991). Recent results from Foley et al. (2002, 2003) have shown, on the basis of Nb/Ta and Zr/Sm ratios in TTG's, that for the formation of these rocks, melting must take place in the amphibolite rather than the eclogite stability field. Their experiments show that komatiitic material, which is more mafic than the present basaltic oceanic crust, and which may be expected to be more abundant for higher mantle temperatures (Nisbet, 1982), would transform into pyroxenite instead of eclogite at high pressure, which they infer to produce basaltic melts upon partial melting, and not TTG-like melts.

Eclogitic xenoliths from cratonic regions often show a depleted nature, indicating that melt has been extracted, and it has been suggested that these are remnants of granitoid formation, complementary to these crustal rocks (e.g. Rollinson, 1997; Barth et al., 2001). Furthermore, oxygen isotope studies on coesite inclusions in diamonds from

eclogite xenoliths from the Guyana Shield suggest interaction of the original rock with sea water similar to modern day hydrothermal alteration of oceanic crust at mid-ocean ridges (Schulze et al., 2003). However theoretical considerations and numerical models have shown that maintaining plate tectonics in a hotter Earth is quite difficult (Vlaar and Van den Berg, 1991; Van Hunen, 2001; Van Thienen et al., 2003c, chapter 4). Adakites, formed by partial melting of a young, hot slab in a subduction zone setting, are sometimes considered as a modern day analogue of TTG's (Martin, 1999), and interpreted as supporting early plate tectonics. Smithies (2000) however showed that adakites and TTG's differ in Mg number and SiO_2 contents, indicating that adakitic melts underwent interaction with mantle peridotite whereas TTG melts (especially pre 3.0 Ga) did not. A more suitable setting for producing TTG's than a subduction zone is therefore melting at the base of a thickened crust (Smithies, 2000). The composition of Phanerozoic Na-rich granitoids formed in this way (e.g. Atherton and Petford, 1993; Johnson et al., 1997) more closely matches the range of composition of Archean TTG's (Smithies, 2000). Alternatively, the intrusion and crystallization of mantle melts in the lower crust may provide a heat source for partial melting of the lower crust (Huppert and Sparks, 1988; Petford and Gallagher, 2001). Other mechanisms proposed in the literature use similar settings. Campbell and Hill (1988) suggested that the heat of a hot asthenospheric upwelling interacting with an existing crust may generate felsic melts, thus producing continental material. Theoretical considerations suggest that both the maximum size and the excess temperature of mantle plumes become smaller in a hotter mantle (McKenzie and Bickle, 1988; Nisbet et al., 1993). However, a mantle plume originating from a separately convecting lower mantle entering the upper mantle may have a much greater size and higher excess temperature (Van Thienen et al., 2003b, chapter 6)), possibly supplying sufficient heat for partial melting of the lower crust. Zegers and Van Keken (2001) proposed that delamination of an eclogitic lower crust and associated extension of the overlying middle and upper crust may allow warmer mantle material to rise to shallower levels and cause crustal melting to produce continental material. They used a numerical model to demonstrate the feasibility of the mechanism and compared results to geological evidence from the Pilbara craton.

In this work we use numerical thermochemical mantle convection models to investigate different geodynamical settings in which partial melting of (meta-)basalt may take place. This is an extension of earlier work (Van Thienen et al., 2003b, chapter 6), in which the dynamics of the self-consistent growth and recycling of thick Archean oceanic crust was investigated. Four different scenarios in which partial melting of (meta-) basalt may take place are investigated in detail: (1) small scale delamination of the eclogitic lower crust, (2) large scale resurfacing by rapid episodic 'subduction' (though not in a plate tectonic sense), (3) heating of the lower part of a thickening crust by the convecting mantle, and (4) heating of the crust from below by a mantle plume. We compare the melting conditions in our models to those inferred for natural TTG's (Winther, 1996), and apply the geochemical constraints that were found for the metamorphic stability field where TTG generation takes place (Foley et al., 2002, 2003). We also investigate the production rates of continental material that is formed by means of this mechanism using numerical models. Finally, we compare the rock associations produced in our models and their geometry to the granite-greenstone associations that are common in Archean terrains and come up

with a new model for the production of these associations which does not require the operation of plate tectonics.

7.2 Model description

The numerical model used is nearly identical to that of Van Thienen et al. (2003b) and chapter 6. Therefore, the model will be described only briefly and the reader is referred to Van Thienen et al. (2003b) and chapter 6 for more information. A single feature has been added to the model: partial melting of basaltic material. This will be described below in section 7.2.4, after a description of the model equations and solid state phase transitions.

7.2.1 Governing equations

Conservation of energy, mass and momentum under the extended Boussinesq approximation (Steinbach et al., 1989; De Smet et al., 1998) for an infinite Prandtl number medium lead to the energy, continuity and Stokes equations (for symbol definitions see Table 7.1):

$$\rho c_p \left(\frac{\partial T}{\partial t} + u_j \partial_j T \right) - \alpha T \frac{dp}{dt} =$$

$$\tau_{ij} \partial_j u_i + \partial_j (k \partial_j T) + \rho_0 H + \frac{\Delta S}{c_p} \frac{dF}{dt} T + \sum_k \frac{\gamma_k \delta \rho_k T}{\rho_0^2 c_p} \frac{d\Gamma_k}{dt} \tag{7.1}$$

$$\partial_j u_j = 0 \tag{7.2}$$

$$\partial_j \tau_{ij} = \partial_i \Delta p - \Delta \rho g_i \tag{7.3}$$

symbol	property	definition	value/unit
c_p	heat capacity at constant pressure		$1250\ \mathrm{Jkg^{-1}K^{-1}}$
F	degree of depletion		
g	gravitational acceleration		$9.8\ \mathrm{ms^{-2}}$
H	radiogenic heat productivity		$\mathrm{Wkg^{-1}}$
p	pressure		Pa
S	melt productivity function		$\mathrm{s^{-1}}$
ΔS	entropy change upon full differentiation		$300\ \mathrm{Jkg^{-1}K^{-1}}$
t	time		s
T	temperature		^{o}C
T_0	non-dimensional surface temperature		$\frac{273}{\Delta T}$
ΔT	temperature scale		2450 ^{o}C
z	depth		m
$z_0(T)$	temperature dependent depth of phase transition		m
α	thermal expansion coefficient		$3 \cdot 10^{-5}\ \mathrm{K^{-1}}$
Γ_k	phase function for transition k	$\frac{1}{2}\left(1 + \sin(\pi \frac{z - z_0(T)}{\delta z})\right)$	

Table 7.1: Symbols definitions and parameter values.

symbol	property	definition	value/unit
δz	depth range of phase transition		m
κ	thermal diffusivity		$10^{-6}\ \mathrm{m^2 s^{-1}}$
ρ_0	reference density		$3416\ \mathrm{kgm^{-3}}$
$\delta\rho$	density difference upon		
	full depletion	$\frac{\partial\rho}{\partial F}$	$-226\ \mathrm{kgm^{-3}}$
$\delta\rho_k$	density increase of		
	phase transition k	$\frac{\partial\rho}{\partial\Gamma_k}$	$\mathrm{kgm^{-3}}$
B_1	diffusion creep prefactor		Pas
B_2	dislocation creep prefactor		$\mathrm{Pa^{n_2}s}$
C_0	cohesion factor		0 Pa
E_1	diffusion creep activation energy		$270 \cdot 10^3 \mathrm{Jmol^{-1}}$
E_2	dislocation creep activation energy		$485 \cdot 10^3 \mathrm{Jmol^{-1}}$
e_{ij}	strain rate tensor	$\partial_j u_i + \partial_i u_j$	$\mathrm{s^{-1}}$
e	second invariant of the		
	strain rate tensor	$[\frac{1}{2} e_{ij} e_{ij}]^{\frac{1}{2}}$	$\mathrm{s^{-1}}$
$f(F)$	composition dependent viscosity prefactor		
n_1	diffusion creep stress exponent		1
n_2	dislocation creep stress exponent		3.25
n_y	yield exponent		10
R	gas constant		$8.341 \mathrm{Jmol^{-1}K^{-1}}$
V_1	diffusion creep activation volume		$6 \cdot 10^{-6} \mathrm{m^3 mol^{-1}}$
V_2	dislocation creep activation volume		$17.5 \cdot 10^{-6} \mathrm{m^3 mol^{-1}}$
$\dot{\varepsilon}$	strainrate		$\mathrm{s^{-1}}$
$\dot{\varepsilon}_y$	yield strainrate		$10^{-15} \mathrm{s^{-1}}$
η	viscosity		Pas
η_0	reference viscosity		10^{20} Pas
η_y	yield viscosity		Pas
σ_n	normal stress		Pa
τ_{ij}	deviatoric stress tensor	ηe_{ij}	Pa
τ	second invariant of		
	the deviatoric stress tensor	$[\frac{1}{2} \tau_{ij} \tau_{ij}]^{\frac{1}{2}}$	Pa
τ_y	yield stress		Pa

Table 7.1: Symbols definitions and parameter values (continued).

The local and time dependent internal heating term H in the energy equation (7.1) is obtained by multiplying a uniform value of $15 \cdot 10^{-12} \mathrm{Wkg^{-1}}$ with the concentration of an incompatible trace element. This trace element has an initial concentration of 1, decays with time (half life 2.5 Gyr) and is fractionated upon partial melting (see below) assuming equilibrium melting for each time step and a distribution coefficient of 10^{-2}.

Evolution of the degree of depletion is described by the following equation:

$$\frac{dF}{dt} = S(p, T, F) \tag{7.4}$$

where S is determined by the parameterization of the melting phase diagram under consideration (De Smet et al., 1998).

All motion is driven by density perturbations described by the equation of state:

$$\Delta\rho = \rho_0 \left\{ -\alpha(T - T_{ref}) + \sum_k \Gamma_k \frac{\delta\rho_k}{\rho_0} + \frac{\delta\rho}{\rho_0} F \right\} \tag{7.5}$$

Three deformation mechanisms account for the creep flow deformation of material. The first two, diffusion creep and dislocation creep, are described by an Arrhenius formulation of the corresponding components of the composite viscosity (Karato and Wu, 1993; Van den Berg and Yuen, 1998):

$$\eta_i = f(F) B_i \exp\left[\frac{E_i + PV_i}{RT}\right] \sigma^{1-n_i} \tag{7.6}$$

with $f(F)$ a composition dependent prefactor (for an explanation of the symbols see Table 7.1). Apart from this prefactor, the parameters of expression (7.6) are based on Karato and Wu (1993) assuming a constant and uniform grainsize of 1 mm. The composition dependent prefactor $f(F)$ has a value of 1 for fertile peridotite and basalt (which have the same viscosity parameters in our models). For depleted peridotite (harzburgite) we apply a prefactor value of 10 for a degree of depletion over 0.05, and a linearly increasing value between $F = 0.005$ and $F = 0.05$ from 1 to 10. This is intended to mimic the effect of dehydration during partial melting on the viscosity (Karato, 1986; Hirth and Kohlstedt, 1996; Mei and Kohlstedt, 2000a,b). For eclogite, the prefactor is set to a value of 0.1, to account for the lower flow stress interpreted by Piepenbreier and Stöckhert (2001) from eclogite microstructures.

The third deformation mechanism included, brittle failure, is parameterized by a yield mechanism approximating the effects of fracturing-like behaviour when the shear stress exceeds a certain yield stress τ_y. We use a formulation of Van Hunen et al. (2002):

$$\eta_y = \tau_y \dot{\varepsilon}_y^{-1/n_y} \dot{\varepsilon}^{(1/n_y)-1} \tag{7.7}$$

The yield stress τ_y, the yield strain rate $\dot{\varepsilon}_y$ and the yield exponent n_y are prescribed parameters (see Table 7.1). The yield stress τ_y is determined from Byerlee's law approximating the normal stress with the lithostatic pressure (e.g. Moresi and Solomatov, 1998):

$$\tau_y = C_0 + \mu \rho_0 g_0 z \tag{7.8}$$

We use a low value of 0.03 for the friction coefficient μ, consistent with results of (Moresi and Solomatov, 1998) for the mobilization of the Earth's lithosphere, and assume the cohesion term C_0 to be of minor importance and set it to 0.

The diffusion and dislocation creep viscosities are inversely added to define an effective ductile creep viscosity (Van den Berg et al., 1993) and the minimum of this value and the local yield viscosity is used for the local effective viscosity.

model	process/setting	domain size (km)	modification	Figure
Mdel	small-scale delamination	600x600	-	7.3a
Mres	resurfacing	600x600	-	7.3b,c
Mtcr	thickened crust	1200x1200	l.m. diapirism suppressed	7.3d
Mdia	l.m. diapirism	1200x1200	-	7.3e

Table 7.2: The range of models focussing on different processes and/or settings, with computational domain size and Figure reference visualizing the process or setting. Modifications of the model conditions relative to the original model Ms from Van Thienen et al. (2003b) (see text) are indicated as well.

7.2.2 Computational methods

The model domain of each experiment is square, with a size of 600 or 1200 km (see Table 7.2). It is discretized using: a) finite elements with a boundary nodal point spacing of 6-12 km for the energy and momentum equations, and b) 200 000 to 400 000 particle tracers, advected with the mantle flow, on which the development of depletion, trace element concentration, and metamorphic phase of basaltic material are evaluated. The vertical boundaries are periodic, and the bottom boundary has a free slip condition. On the top boundary, the vertical velocity is prescribed as a function of melt productivity, as will be described below, to allow the production of crust at the surface. The horizontal, tangential stress component is set to zero. The temperature on the top boundary is set to 0^oC. On the bottom boundary, a temperature consistent with the initial condition (see section 7.2.7) is prescribed.

7.2.3 Solid state phase transitions

Mantle phase transitions in our model are composition dependent and are accounted for in the energy equation (7.1), and the resulting density effects are included in the equation of state (7.5), which enters the buoyancy term of the momentum equation (7.3). Parameters of the phase transitions are listed in Table 7.3. The transition of basalt into eclogite is treated differently. Basalt is transformed into heavier eclogite upon reaching depths in excess of 30 km in our model. The kinetics of this transition are approximated assuming a constant relaxation time for the transition of 1.25 Myr. The depth of 30 km (0.9 GPa) we use is somewhat less than the depth of about 40 km (1.2 GPa) that Hacker (1996) states as the minimum pressure of basalt to eclogite transformation. However, as we are dealing with melt products in a mantle which is hotter than the present, their composition may be more MgO-rich (more towards komatiitic composition) than present day mid ocean ridge basalt (Nisbet, 1982). Experiments of Green and Ringwood (1967) have shown that the transition may occur at lower pressures and higher temperatures in MgO-rich rocks. Furthermore, lower pressure phase assemblages (above 0.7-0.8 GPa) may also contain garnet (Green and Ringwood, 1967; Ito and Kennedy, 1971; Hacker, 1996), thus raising the bulk density above that of the original basaltic phase assemblage. We do not

transition	material	P_0 (GPa)	T_0 (K)	γ (Pa/K)	δz (km)	$\frac{\delta\rho}{\rho_0}$
400	peridotite	13.4	1756	$3 \cdot 10^6$	50	0.05
400	basalt	12.5	1747	$3 \cdot 10^6$	150	0.10
670	peridotite	22.4	1854	$-2.5 \cdot 10^6$	50	0.05

Table 7.3: Parameters of the phase transitions used in the models. The first column indicates the approximate depth of the transition. P_0 and T_0 are the reference temperature and pressure for the phase transition, defining it in combination with the Clapeyron slope γ. The column marked δz indicates the depth range over which the transition is smeared out in the model and the last column gives the relative density contrast of the phase transition.

consider phase boundary topography due to temperature effects, since we expect this to be dominated by kinetic effects because of the relatively low Clapeyron slope of about 1 MPa/K (Philpotts, 1990).

7.2.4 Partial melting

Partial melting of fertile mantle peridotite may produce a spectrum of melt compositions, ranging from tholeiitic to komatiitic. In general, higher melting pressures and/or greater degrees of melting meaning higher temperatures produce melts that are more MgO-rich, so more to the komatiitic side of the spectrum (Philpotts, 1990). Partial melting of basaltic material may also produce a range of melt compositions, depending on the conditions of melting. This melting behaviour is simplified in our models, where the composition field defines three different basic types of materials: mantle peridotite, basalt and felsic material. These terms are used here to describe larger groups of rocks than their specific geological definitions. *Basaltic* materials are understood here to include all melt products of mantle peridotite, regardless of melting conditions, and the term *felsic* materials is used to indicate all melt products of basaltic material. Mantle peridotite and basalt have an extra component to their composition, which is the *degree of depletion*. Partial melting is modelled as an (irreversible) increase in this degree of depletion F, which is defined here as the mass fraction of melt produced from an initially unmelted material control volume of mantle peridotite or basalt. Since no material is actually removed in our model, the volumes of depleted residual material are somewhat overestimated (De Smet, 1999). The source function S in (7.4) describes the distribution of the rate of partial melting, applying a simple parameterization of the melting phase diagram of mantle peridotite (De Smet et al., 1998). We use third order polynomial parameterizations of the solidus and the liquidus of mantle peridotite, based on Herzberg and Zhang (1996), down to a depth of 400 km (see Figure 7.1), assuming that melt produced below this depth is not segregated. Our isobaric melting curve, which is based on data presented by Jaques and Green (1980), is linear (see De Smet et al., 1998). A similar approach is used for partial melting of basaltic material. Since in our models, all melts that are produced are assumed to migrate

to the surface (see section 7.2.5), we can also assume that the crustal material produced by solidification at the surface becomes hydrated by contact with surface water. This is supported by isotope studies on coesite inclusions in diamonds in eclogite xenoliths from the Guyana Shield (Schulze et al., 2003), which indicate significant interaction with water. We therefore use a hydrous solidus and liquidus in our model experiments, based on data from Green (1982), see Figure 7.1. We use the same linear melting function for the partial melting of basalt as that used for peridotite.

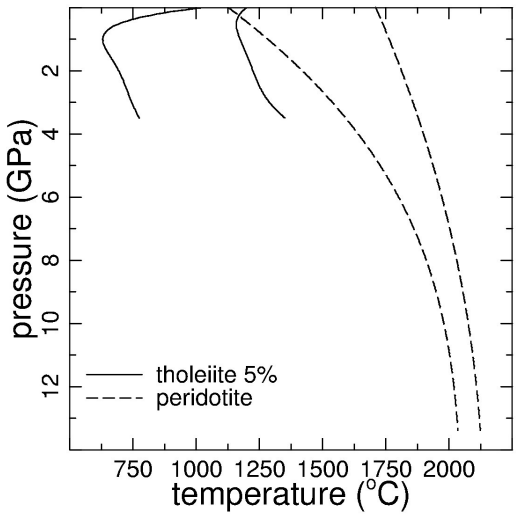

Figure 7.1: Solidus and liquidus parameterizations used in the models for basalt/eclogite (solid curves) and peridotite (dashed curves). The basaltic curves are based on experimental results from a hydrated (5 percent water by weight) tholeiite (Green, 1982). The peridotite curves are based on Herzberg and Zhang (1996).

7.2.5 Crustal growth

An important feature of the model is the self-consistent growth of crust. All melt that is produced in the model domain is assumed to migrate to the surface on time scales much shorter than the characteristic time scales of the model. We therefore let all melt that is produced flow into the model through the top boundary above the region where the melt was formed. When both basaltic and felsic crust is being produced, the inflowing material is a mixture of these two components, defined by different tracer composition values, in relative proportions corresponding to the respective amounts of melt being produced. The trace element concentrations of inflowing basalt and felsics are a function of the fractionation during partial melting of the respective source rocks.

7.2.6 Metamorphic phase stability fields

Trace element ratios (Nb/Ta and Zr/Sm) in TTG's indicate that these rocks have been formed by partial melting of a meta-basalt in the amphibolite rather than the eclogite stability field (Foley et al., 2002, 2003). This is based on the modelling of trace element distribution, which indicates that amphibole must be present in the source rock and rutile, common in Archean eclogite xenoliths (Rudnick et al., 2000), must be absent. It is therefore important to monitor the pressure and temperature conditions under which partial melting takes place in our experiments. Figure 7.2 shows the metamorphic phase diagrams for three different compositions. We have included three different compositions because of the uncertain nature and variability of the dominant rock type in early oceanic crust. Basaltic crust created at a mid-ocean ridge will be thicker for higher temperatures (Vlaar and Van den Berg, 1991), and have a higher MgO content (Nisbet, 1982) than present MORB-like compositions. However, in an alternative geodynamic regime like that which is modelled in this work, production of crust does not take place due to partial melting of focused upwelling mantle in a ridge setting, but by stacking of extrusive units produced at many locations from partial melting of the convecting mantle. Due to the presence of pre-existing crust and a depleted root, partial melting takes place at greater depths, which tends to increase the MgO content (Philpotts, 1990), and to lower degrees of melting, which counteracts this effect. Therefore, the dominant composition of crust produced by partial melting of mantle peridotite is expected to be somewhere in the wide range between a basaltic and a komatiitic composition, and we will include all three phase diagrams of Figure 7.2 in the discussion of the results of the numerical models.

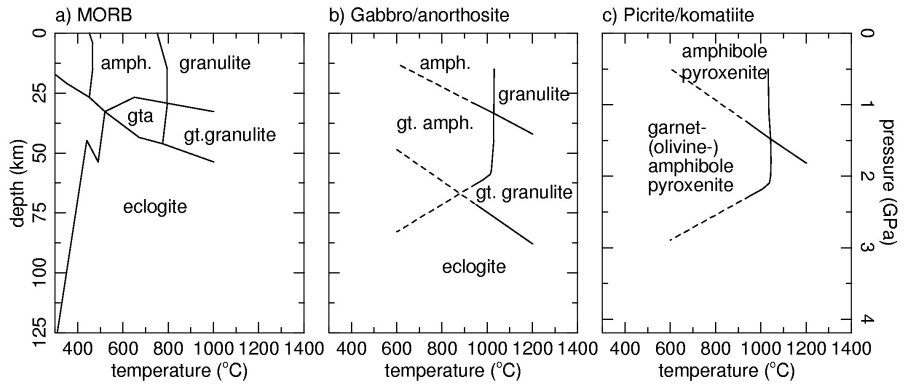

Figure 7.2: Metamorphic phase diagrams for different magmatic rocks, which may be expected in Archean oceanic crust. a) Mid-Ocean Ridge Basalt, from Hacker et al. (2003). *amph.* indicates amphibolite, *gta* is garnet-amphibolite, and *gt. granulite* is garnet granulite. b) Gabbro/anorthosite (Green and Ringwood, 1967; Foley et al., 2003). c) Picrite/Komatiite. Data from experiments on Gorgona komatiite by Foley et al. (2003).

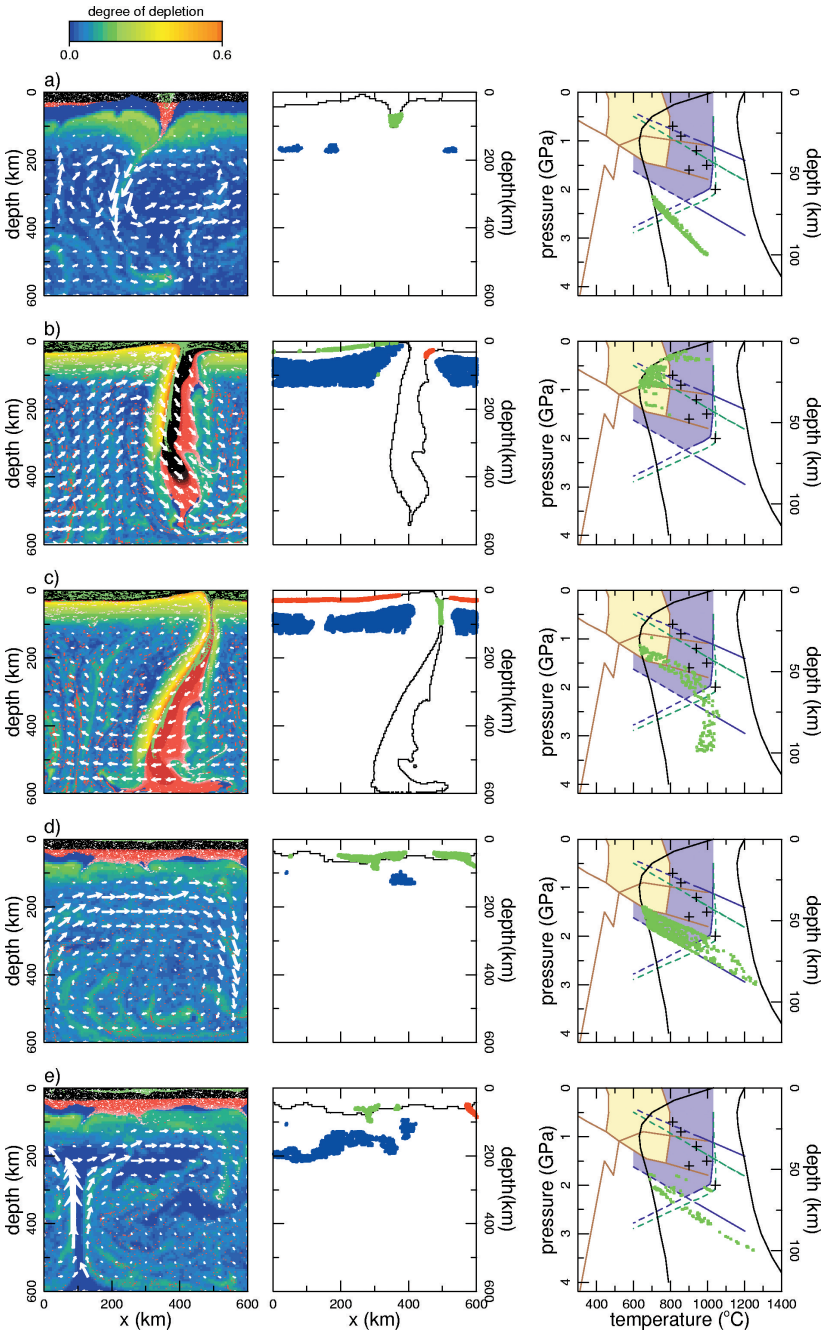
degree of depletion
0.0
0.6
a)
b)
c)
d)
e)
depth (km)
depth(km)
pressure (GPa)
x (km)
temperature (°C)

Figure 7.3: (previous page) Partial melting of metabasalt in five different geodynamical settings. The left hand side frames show the composition field, with the colour scale from blue to orange indicating the degree of depletion of peridotite. Black indicates basalt, red is eclogite, and the colour range in between indicates material in the transition stage. Eclogite becomes lighter red as it is more depleted. Greenish crustal material is the product of (meta-) basalt melting. The middle frames show basaltic particle tracers that undergo partial melting in red and green, and melting peridotite in blue. The green tracers are also shown in the right hand side frames, which show the location of partial melting of metabasalt in p,T-space. The phase diagrams represented in Figure 7.2 are included, and the regions that produce Nb/Ta and Zr/Sm ratios consistent with natural TTG's are indicated in yellow (MORB) and purple (gabbro/anorthosite). The inferred melting conditions of some natural TTG's (Winther, 1996) have been included as black crosses, and solidus and liquidus used are indicated by black curves. Note that the frames in the right column have a different depth scale than the other frames. a) Small scale delamination of the lower crust (Mdel). b) Partial melting of a newly produced lower crust associated with a resurfacing event (Mres). c) Partial melting in a 'subducting' crust during a resurfacing event (Mres). d) Partial melting of the base of a thickened crust (Mtcr). e) Lower mantle diapirism (Mdia). Frames d) and e) only show 1/4 of the complete computational domain of 1200x1200 km.

Figure 7.2a shows the diagram for a MORB composition (simplified from Hacker et al., 2003). The results of Foley et al. (2002) show that partial melting of metabasalts in the (garnet-) amphibolite stability field produces TTG melts. For a MORB composition, this is at depths less than 50 km at temperatures between approximately 450 and 800^oC.

For a gabbroic/anorthositic composition (Figure 7.2b, from a diagram of Foley et al. (2003) based on data from Green and Ringwood (1967)), the amphibolite stability field, and therefore the TTG production field, is larger, extending up to temperatures of about 1000^oC and depths of about 75 km (note that the dashed lines are extrapolations of the phase boundaries indicated by solid lines).

No amphibolite is formed for picritic/komatiitic compositions (Figure 7.2c, from Foley et al., 2003), and these rocks do not produce TTG-like melts under any conditions during partial melting, but basaltic liquids instead.

7.2.7 Initial conditions

The initial conditions for the present experiments are derived from model Ms in Van Thienen et al. (2003b) and chapter 6. This original model was started with a cool (subsolidus) mantle with an extreme heating rate of $250 \cdot 10^{-12} Wkg^{-1}$, in order to produce a hot and differentiated initial state for our experiments. This extreme internal heating value was reduced to a normal early Earth value of $15 \cdot 10^{-12} Wkg^{-1}$ after 30 km of basaltic crust had been produced. In the present experiments, we use a snapshot of the entire domain (1200x1200 km) or part of the domain (600x600 km) as a starting condition, see

Table 7.2. Due to the prescribed periodic boundary condition on the vertical boundaries, the latter case results in inconsistencies, since the new boundaries were previously unconnected and therefore did not have the same temperature and velocities. However, these are small and do not significantly influence the solution. In contrast with the present experiments, the original model did not include partial melting of basalt. Therefore, the present experiments show an initial pulse of melting of basaltic material where the temperature is above the basalt solidus. In one experiment (Mctr, see Table 7.2), the generation of a lower mantle diapir is suppressed by increasing the density contrast over the γ-olivine-perovskite phase transition. In every other respect, this model is the same as model Mdia.

7.3 Results

7.3.1 Geodynamical settings

In this work we investigate the partial melting of (meta-)basalt in five different geodynamical settings, associated with different processes that may have been important in the production and recycling of oceanic crust in the early Earth, and which have been described in more detail by Van Thienen et al. (2003b) and in chapter 6. The left hand side and middle frames of Figure 7.3 illustrate all five processes, showing the composition field. In the left hand frames, the colour scale from blue to orange indicates the degree of depletion of peridotite. Basaltic/eclogitic (black/red) and felsic (green) tracers are included. Depleted metabasalt has a lighter red colour. Arrows indicate the instantaneous flow field. The middle frames show the contours of the crust in black, with regions of partial melting of peridotite in blue and partial melting of (meta-) basalt in red and green.

The first process is small scale delamination of the lower crust (Figure 7.3a).

Partial melting in the upwelling limb of a small scale mantle circulation may locally add material to the crust, which becomes thicker. The lower part of the crust may become involved in the circulation. At first this is passive entrainment, but when sufficient basalt has turned into eclogite the involvement becomes active. Partial melting of metabasalt takes place in the tip of the downwelling material, indicated by the green spot in the middle frame.

The second process is large scale resurfacing, shown in Figure 7.3b,c. In this process, a local anomalous thickening of the crust, for example caused by the addition of material by a mantle plume, may become gravitationally unstable when a large part of the (lower) crust has turned into eclogite. This may trigger the entire crust to sink into the mantle on a very short time scale (about 2 million years). New crust is produced by partial melting of upwelling mantle material. Two settings for partial melting of (meta-) basalt can be indicated here. Figure 7.3b shows partial melting, indicated by the green colour in the middle frame, at the base of the freshly produced crust that replaces the material which is sinking into the mantle. The required heat is supplied by upwelling mantle material associated with the resurfacing event. In Figure 7.3c, partial melting takes place in the sinking crustal material itself, indicated by the green colour in the middle frame.

Figure 7.3d shows the third process, which is the partial melting of a locally thickened

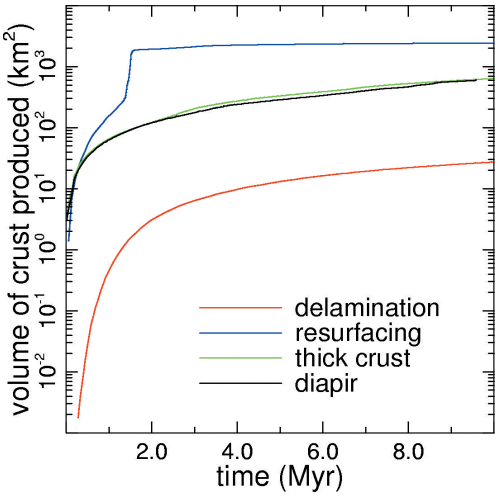

Figure 7.4: 2-D volumes of felsic material produced by partial melting in the different models. Volumes are normalized to a 600 km domain for larger models.

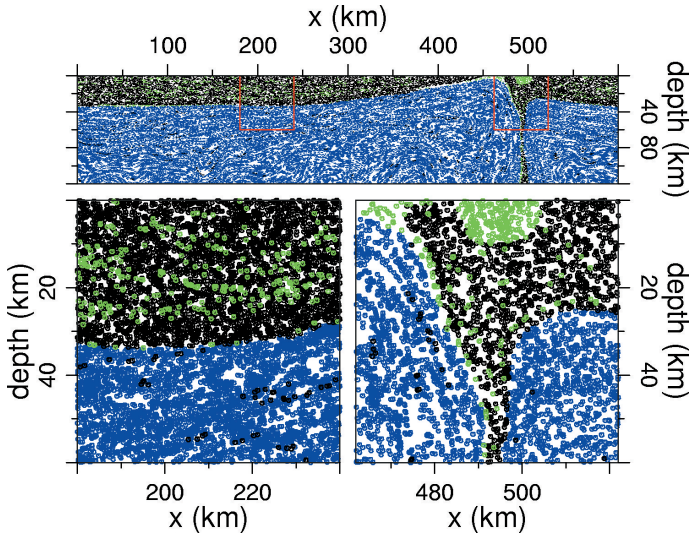

Figure 7.5: Zoom-in on the crust of model Mtcr as shown in Figure 7.3c. (Meta-)basaltic tracers are indicated in black, felsic tracers in green, and (both depleted and fertile) peridotitic tracers in blue. Two red squares in the top panel indicate the locations of the zoom-ins of the lower frames.

crust. Due to successive stacking of basaltic extrusives, the crust locally extends to about 80 km depth at temperatures above the hydrous basalt solidus. Penetration of a mantle diapir into the upper mantle as a heat source for melting at the base of the crust is shown in Figure 7.3e.

7.3.2 Conditions of partial melting

The p,T-conditions under which partial melting of metabasalt takes place in the different geodynamical settings with respect to the metamorphic phase boundaries (see Figure 7.2) are indicated in the right hand side frames of Figure 7.3. The p,T-conditions of melting basaltic tracers are indicated in green, and the corresponding locations are indicated in green in the middle frames (melting tracers not indicated in the p,T diagrams are shown in red). These results show that if we assume a MORB-like composition (brownish phase boundaries in Figure 7.3) for the basaltic crust that is partially melting in our experiments, TTG-like melts formed in the amphibole stability field consistent with observations of Nb/Ta and Zr/Sm ratios in natural TTG's can be produced in two of the geodynamical settings, both associated with large-scale resurfacing (see Figure 7.3b,c, where the yellow region indicates the (garnet-) amphibolite stability fields). The melting conditions at the base of the newly produced crust correspond to the shallow conditions inferred for natural TTG's by Winther (1996), indicated by black crosses in the right hand frames. In the sinking crust (Figure 7.3c), conditions correspond to the deepest conditions for natural TTG's inferred by Winther (lowest two crosses in the right hand frame). In the other settings, melting takes place at levels that are too deep for amphibolite stability, well into the eclogite field. For material with a gabbroic/anorthositic composition (purple phase lines), the stability field of (garnet-) amphibolite (purple shaded area, partially overlapping with the yellow MORB region) is extended relative to MORB. The two settings associated with the resurfacing event again produce TTG melts. Partial melting of the lower thickened crust in either the presence (Figure 7.3d) or absence (Figure 7.3e) of a mantle diapir may also produce TTG melts, but the uncertain location of the extrapolated boundary of the amphibole stability field makes this questionable. The small-scale delamination setting does not produce TTG melts in the amphibole stability field consistent with natural TTG's. More mafic material, represented by the greenish phase boundaries in Figure 7.3 for picrite/komatiite, show most melting in the (garnet-) pyroxenite fields, producing basaltic melts.

7.3.3 Production rates of continental material

Figure 7.4 shows the 2-D volume of felsic material produced in the different geodynamical settings listed in Table 7.2 and shown in Figure 7.3. The values for 1200x1200 km models (Mtcr and Mdia) have been normalized to correspond to the 600x600 km domain of the other models. It is clear from this figure that the crustal production rates range over orders magnitude for the different processes. A single small-scale delamination (see Figure 7.3a) produces about $30\mathrm{km}^2$ of crust in 10 million years, whereas partial melting of metabasalt associated with a resurfacing event (see Figure 7.3b,c) produces nearly

$2000\mathrm{km}^2$ in less than 2 million years. This corresponds to equivalent felsic layers spread out over the entire domain width of 50 m and 3.3 km, respectively. Another important point of Figure 7.4 is the near coincidence of the curves of models Mtcr (thickened crust) and Mdia (lower mantle diapirism). This indicates that although much hot lower mantle material is introduced into the upper mantle in model Mdia and not in model Mtcr, it does not pass this heat on directly to the lower crust to allow it to melt. The diapir head spreads out in the upper mantle and does not reach depths less than 100 km (consistent with the maximum depth of 90 km attained by a numerical model diapir in similar thermal and identical rheological conditions in Van Thienen et al., 2003a, and chapter 8), and does not reach shallower levels where crustal material is present.

7.3.4 Distribution of felsic material in the crust

In order to link the results of our numerical experiments to field observations on Archean cratons, we examine the distribution of felsic material in the crust and its association with basaltic material. Figure 7.5 illustrates the distribution of basaltic and felsic material in the crust of model Mtcr (see Figure 7.3c) by showing all individual particle tracer compositions (basaltic: black, felsic: green, peridotitic: blue) in different regions of the domain. Zoom-ins of two settings in which TTG-melts are produced by partial melting of (meta-)basalt, indicated by red squares in the top panel, are presented in the lower frames. The left panel shows a crustal section associated with the partial melting of young lower crust in a resurfacing setting. Although basaltic material dominates the crust, a significant amount of felsic material is interspersed throughout the crust. In our model, this is produced by the successive stacking of basaltic and felsic extrusives, but in a similar setting in the Earth, intrusives are also possible. The lower right panel of Figure 7.5 shows a zoom-in of a crustal section associated with 'subducting' basaltic crust. This image is quite different from the previous, since in the downwelling part only partial melting of metabasalt is taking place, and not of peridotite. This results in the exclusive production of felsic crust without any associated basaltic crust. In our model, a felsic body of about 20 km width and 10 km depth is produced.

7.4 Discussion

The results of our modelling experiments as shown in Figure 7.3 indicate that the production of TTG lavas in the amphibole stability field in a hot Archean mantle is more likely to take place in settings associated with a resurfacing event than in association with a mantle plume or small scale delamination of the lower crust. However, due to the simplifications made in our numerical model, one possibly important agent of heat transfer is not included in our experiments. The emplacement of a basaltic liquid (both the high temperature and the latent heat effect of solidification) may cause significant amounts of partial melting in the lower amphibolitic crust (Huppert and Sparks, 1988; Petford and Gallagher, 2001). Therefore, specifically mantle diapirism may still be important because it may generate large amounts of basaltic melt (see the blue tracers in the middle frame of

Figure 7.3e, indicating peridotite melting), which may in this way cause partial melting in the lower crust. It may also play an additional role in the partial melting of the newly produced crust associated with a resurfacing event in Figure 7.3b. However, because of the smaller length scales of porous 2-phase flow compared to flow of mantle material (Scott and Stevenson, 1984, find magma soliton wave lengths of a few kilometers for plausible estimates of parameter values, which require a spatial resolution of an order of magnitude smaller to be accurately resolved numerically), inclusion of realistic melt segregation through multi-phase flow in upper mantle scale numerical models is a major computational challenge at the moment.

Because the resurfacing events as shown in Figure 7.3b,c are episodic, the production of felsic material in the associated settings is episodic as well. This is consistent with geological evidence, which indicates that the addition of felsic material to cratons was an episodic process, for example in the Pilbara craton (Smith, 2003) and the Kaapvaal craton (Anhaeusser and Walraven, 1999).

On average, Archean cratons consist of 60 percent granitoid gneiss, 30 percent massive granitoid plutons and 10 percent greenstone belts (Goodwin, 1991). These greenstone belts generally consist of successions of major (ultra)mafic and minor felsic supracrustal rocks, and have *preserved* thicknesses of 5-20 km (Condie, 1994). The massive granitoid plutons, on the other hand, are units of tens to over 100 km diameter that consist of granitoids, the early and mid-Archean cases typically belonging to the TTG suite and later granitoids being dominated by potassic granites (Goodwin, 1991). The greenstone association may correspond well to the type of crust produced by partial melting of the lower part of newly produced crust in association with a resurfacing event, as can be seen in the lower left panel of Figure 7.5. The granitoid plutons correspond well to the large volume of felsics that are produced above a sinking crust in a resurfacing setting without any associated basalts, as shown in the lower right panel of Figure 7.5. Zegers et al. (1999) did radiometric dating of felsic intrusives and supracrustal (greenstone belt) rocks from the eastern Pilbara (> 3 Ga), and found two distinct periods of about 50-80 Myr in which both large batholiths and supracrustal rocks were produced. This shows that the coeval production of these two types of rock associations may be consistent with geological observations. Although greenstone belts appear to have been formed in a variety of settings, a number of them show oceanic assemblages (Kimura et al., 1993; Nijman et al., 1998; Kerrich et al., 1999). The setting in which the greenstone-like succession is produced, forming the new crust in a resurfacing event, can also be considered an oceanic environment. The short time scale on which the crust interpreted as greenstone belt in our model is produced contrasts with the fact that the age of individual units within a greenstone belt may show an age range of 300 Myr (Thurston, 1994). Therefore, it may be more realistic to interpret the crustal segment produced in the resurfacing event as a single unit of a greenstone belt, to which new material may be added later by similar or other processes.

On the basis of these results, we propose that resurfacing events may have played an important role in the early formation of Archean cratons. The mechanism coevally forms both greenstone-like successions and massive volumes of felsic melt, which may form large plutons. The TTG's produced have low Nb/Ta and high Zr/Sm ratios as a result of

melting in the amphibolite stability field, consistent with analyses of Archean TTG rocks (Foley et al., 2002). Furthermore, this mechanism does not require the operation of plate tectonics, which is often invoked to explain Archean geology in general (e.g. De Wit, 1998) and greenstone belt formation specifically (see Table 5 of Polat et al., 1998), but against which strong physical arguments have been published for a hotter mantle (Vlaar, 1986; Vlaar and Van den Berg, 1991; Van Thienen et al., 2003c, chapter 4).

Our model results are also relevant for Venus. Crater count studies indicate that a global resurfacing took place on Venus around 500 million years before present (Schaber et al., 1992). Resurfacing may have taken place episodically on Venus (Turcotte, 1995; Fowler and O'Brien, 1996), possible by periodic plate tectonics (Solomatov and Moresi, 1996) or by the resurfacing mechanism that is applied in this work (Van Thienen et al., 2003b, chapter 6). Venus is a dry planet, although it may have been somewhat wetter in its earlier history, possessing a fraction of $x \cdot 10^{-3}$ of the terrestrial oceans (Campbell and Taylor, 1983; Nimmo and McKenzie, 1998). Since the production of granitoids requires water (Campbell and Taylor, 1983), the resurfacing mechanism would not produce granitoids on Venus as it does in our models applied to Earth, in line with the absence of evidence for significant amounts of silicic crust on Venus.

7.5 Conclusions

The model results show partial melting of metabasalt at two distinct settings associated with rapid resurfacing, at the base of newly produced basaltic crust and in the necking part of a 'subducting' old crust, takes place in the amphibolite stability field when assuming a basaltic or gabbroic crustal composition. In the other settings that were investigated, which are small scale delamination of the lower crust, melting at the base of a anomalously thick crust and melting associated with a lower mantle diapir, partial melting of metabasalt generally takes place under uncertain metamorphic conditions or in the eclogite stability field. Since the former type of melting produces TTG melts with Nb/Ta and Zr/Sm ratios consistent with geochemical observations, and the latter does not, we suggest that partial melting of metabasalt associated with resurfacing events may have been an important agent in the production of continental material during the early history of the Earth. Furthermore, the configuration of the rock associations produced in our model resembles Archean granite-greenstone terrains, and we therefore propose that the resurfacing mechanism may have played an important role in the generation of (some of) these granite-greenstone associations found on Archean cratons. The resurfacing mechanism may also have been active on Venus, but due to the dryness of this planet, it probably did not produce large volumes of continental material.